

## Article

# Analysis of Short-Term Heavy Rainfall-Based Urban Flood Disaster Risk Assessment Using Integrated Learning Approach

Xinyue Wu <sup>1</sup>, Hong Zhu <sup>1,2,\*</sup>, Liuru Hu <sup>3,4</sup> , Jian Meng <sup>1</sup> and Fulu Sun <sup>1</sup>

<sup>1</sup> School of Earth Sciences and Engineering, Institute of Disaster Prevention, Beijing 101601, China; wuxinyue10011999@163.com (X.W.)

<sup>2</sup> Institute of Disaster Prevention, College of Ecology and Environment, Beijing 101601, China

<sup>3</sup> College of Geomatics, Xi'an University of Science and Technology, Xi'an 710054, China

<sup>4</sup> Departamento de Ingeniería Civil, Escuela Politécnica Superior de Alicante, Universidad de Alicante, P.O. Box 99, E-03080 Alicante, Spain

\* Correspondence: zhong@cidp.edu.cn

**Abstract:** Accurate and timely risk assessment of short-term rainstorm-type flood disasters is very important for ecological environment protection and sustainable socio-economic development. Given the complexity and variability of different geographical environments and climate conditions, a single machine learning model may lead to overfitting issues in flood disaster assessment, limiting the generalization ability of such models. In order to overcome this challenge, this study proposed a short-term rainstorm flood disaster risk assessment framework under the integrated learning model, which is divided into two stages: The first stage uses microwave remote sensing images to extract flood coverage and establish disaster samples, and integrates multi-source heterogeneous data to build a flood disaster risk assessment index system. The second stage, under the constraints of Whale Optimization Algorithm (WOA), optimizes the integration of random forest (RF), support vector machine (SVM), and logistic regression (LR) base models, and then the WRSL-Short-Term Flood Risk Assessment Model is established. The experimental results show that the Area Under Curve (AUC) accuracy of the WRSL-Short-Term Flood Risk Assessment Model is 89.27%, which is 0.95%, 1.77%, 2.07%, 1.86%, and 0.47% higher than RF, SVM, LR, XGBoost, and average weight RF-SVM-LR, respectively. The accuracy evaluation metrics for accuracy, Recall, and F1 Score have improved by 5.84%, 21.50%, and 11.06%, respectively. In this paper, WRSL-Short-Term Flood Risk Assessment Model is used to carry out the risk assessment of flood and waterlogging disasters in Henan Province, and ArcGIS is used to complete the short-term rainstorm city flood and waterlogging risk map. The research results will provide a scientific assessment basis for short-term rainstorm city flood disaster risk assessment and provide technical support for regional flood control and risk management.

**Keywords:** flood; risk assessment; machine learning; factor analysis; integrated model



**Citation:** Wu, X.; Zhu, H.; Hu, L.; Meng, J.; Sun, F. Analysis of Short-Term Heavy Rainfall-Based Urban Flood Disaster Risk Assessment Using Integrated Learning Approach. *Sustainability* **2024**, *16*, 8249. <https://doi.org/10.3390/su16188249>

Academic Editor: Faccini Francesco

Received: 10 June 2024

Revised: 7 September 2024

Accepted: 11 September 2024

Published: 22 September 2024



**Copyright:** © 2024 by the authors. Licensee MDPI, Basel, Switzerland. This article is an open access article distributed under the terms and conditions of the Creative Commons Attribution (CC BY) license (<https://creativecommons.org/licenses/by/4.0/>).

## 1. Introduction

In recent years, extreme weather events have become more frequent and severe. The escalation in extreme weather presents significant challenges to both ecological environments and socio-economic development [1,2]. Flooding, recognized as one of the most devastating natural disasters [3–5], has a profound impact on people's lives and property. Due to global climate change, financial losses from flooding have risen markedly [6,7], and urban storm waterlogging disasters have become frequent. Consequently, conducting short-term storm-type urban flood risk assessments is crucial to help city managers prioritize flood resilience measures.

Current flood risk assessment methodologies are generally categorized into five types [8]: historical disaster mathematical statistics, scenario simulation, coupling of remote sensing and geographic information systems (GIS), multi-criteria decision analysis (MCDA), and machine learning. The Historical Disaster Mathematical Statistics Method [9]

utilizes mathematical statistics to identify patterns in disaster occurrences [10]. Although this method is simple to calculate, it depends on long-term basic hydrological observation data series for analysis. The assessment results can reflect the overall regional flood risk but fail to illustrate spatial differences in risk. The scenario simulation method, based on hydrology and hydraulics principles, builds flood simulation models [11,12] to simulate the extent and impact of floods under various scenarios. However, the required data for modeling, which may include encrypted information such as the design and capacity of urban drainage networks, are often difficult to obtain, and the modeling process is complex. Thus, this method is unsuitable for large-scale areas. The coupled remote sensing and GIS method extracts information from remote sensing images (e.g., extent of inundation, location of affected bodies) and inputs it into GIS software for spatial analysis, visualizing the spatial distribution of flood hazards [13]. Nevertheless, optical remote sensing images are prone to cloud cover, leading to data gaps [14]. Although microwave remote sensing can penetrate clouds, it suffers from incomplete image coverage [15]. MCDA, grounded in flood risk assessment theory, adapts key indicators to the regional context to develop a risk assessment framework [16,17]. However, reliance on traditional mathematical and statistical methods may compromise the objectivity in determining indicator weights [18]. Recently, the use of computational models and high-performance computing technologies has popularized machine learning (ML) methods in flood assessment. Considering the complex, nonlinear nature of flooding with significant spatial and temporal variability [19], ML employs historical data to construct numerical models that accurately represent flooding dynamics. This approach offers higher accuracy and performance than physical models, while simplifying model construction to enhance flexibility and efficiency in practical applications [20]. ML methods demonstrate superior accuracy compared to traditional statistical models [21]. Commonly utilized ML models in flood risk assessment include Artificial Neural Networks (ANNs) [22], support vector machines (SVMs) [23], random forests (RFs) [24], and logistic regression (LR) [25] with XGBoost [26], which have yielded notable results in flood risk assessment. However, a single ML model may suffer from overfitting in flood risk assessment [27] and the stability of model generalization can be challenging under different scenarios [28]. Consequently, integrated models have been developed to enhance flood risk assessment. Integration methods such as Bagging, Boosting, Random Subspace (RS), Stacking, and Blending have been applied in flood hazard risk analysis [29–33]. Bagging and Boosting reduce the instability or bias of individual models by combining similar types (e.g., decision trees), while RS, Stacking, and Blending methods integrate various base models. The results indicate that Bagging significantly improves model performance compared to individual ML models, whereas RS does not enhance performance [33]. Conversely, Stacking and Blending methods significantly improve the accuracy, true rate, and AUC of the models, with the Blending method performing best in terms of these performance indicators [29]. The strengths of integrated models lie in their versatility and robustness, with many empirical studies showing that these methods often outperform single ML models [34]. However, integrated learning methods applied to flood risk assessment analysis still face challenges such as susceptibility to overfitting and difficulty in parameter tuning.

Therefore, this study integrates heterogeneous data from multiple sources and proposes a short-term storm-based urban flood risk assessment method under an integrated learning model. The main contributions of this study include:

- (1) From the perspectives of hazard, exposure, and vulnerability, a total of 21 initial indicators were selected. These indicators were reduced to 16 by eliminating redundant factors using the Pearson method, thereby constructing a short-term storm-type urban flood risk assessment index system.

- (2) Integrating the machine learning methods of RF, SVM, and LR, the whale optimization algorithm (WOA) is employed to calculate the weight of the integrated model. The objective is to minimize the mean square error (MSE) between the estimated and actual flood risk values, resulting in the development of the WRS – Short Term Flood Risk

Assessment Model. This model facilitates the completion of a high-resolution (1km x 1km) short-term rainstorm urban waterlogging risk assessment map.

## 2. Study Area and Data Sources

### 2.1. Study Area

Henan Province (31°23~36°22 N, 110°21~116°39 E) is situated in the central-eastern part of China and spans the middle and lower reaches of the Yellow River. Covering an area of 167,000 square kilometers, it has a resident population of 98.15 million, with an overview of the study area depicted in Figure 1. The topography of Henan is characterized by high elevations in the west and lower elevations in the east, bordered by mountains to the north, west, and south, with the Huanghuaihai Plain centrally and easterly located. The varied terrain includes plains, basins, mountains, hills, and watersheds, extending across four major river basins: the Hai, Yellow, Huai, and Yangtze Rivers. The climatic regime is primarily influenced by the westerly winds, featuring a warm-temperate to subtropical, humid to semi-humid monsoon climate. This climate is noted for its four distinct seasons, concurrent rainfall and heat, and complex and diverse nature, often accompanied by frequent meteorological disasters [35]. On 20 July 2021, Henan Province experienced an extreme heavy rainfall event. According to the Henan provincial government, the event impacted 14.78 million individuals, resulting in 398 deaths or missing persons, and direct economic losses estimated at approximately CNY 12 billion [36].

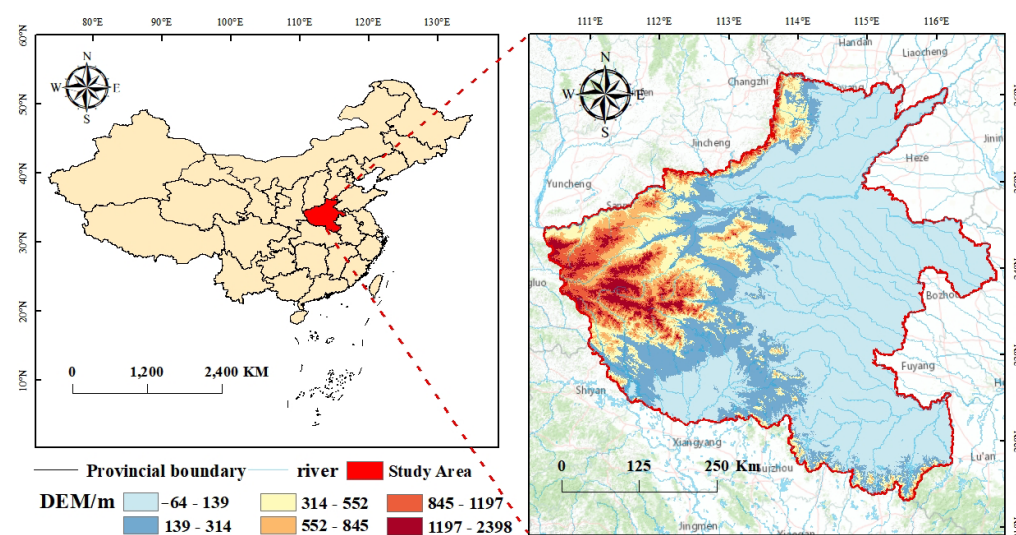


**Figure 1.** Schematic diagram of experimental area.

### 2.2. Data Sources

#### 2.2.1. Data Acquisition of Flood Disaster Sample Points

Pre-disaster and post-disaster Sentinel-1 images from 1 July to 19 July 2021, and from 20 July to 10 August 2021, were used for the experiment. The identification of the affected surface extent of urban flooding was accomplished using the U-Net++ network [37]. In Zhengzhou and Xinxiang cities, 250 flooded and 350 non-flooded points were randomly selected for the training set, and 107 flooded and 150 non-flooded points comprised the test set. To further verify the model's generalizability, 107 flooded and 150 non-flooded points were randomly selected to construct the validation set in other regions of Henan Province (excluding Zhengzhou and Xinxiang cities). Ultimately, the distribution among the training set, test set, and validation set was 7:3:3, and the distribution of flooding sample points is shown in Figure 2.

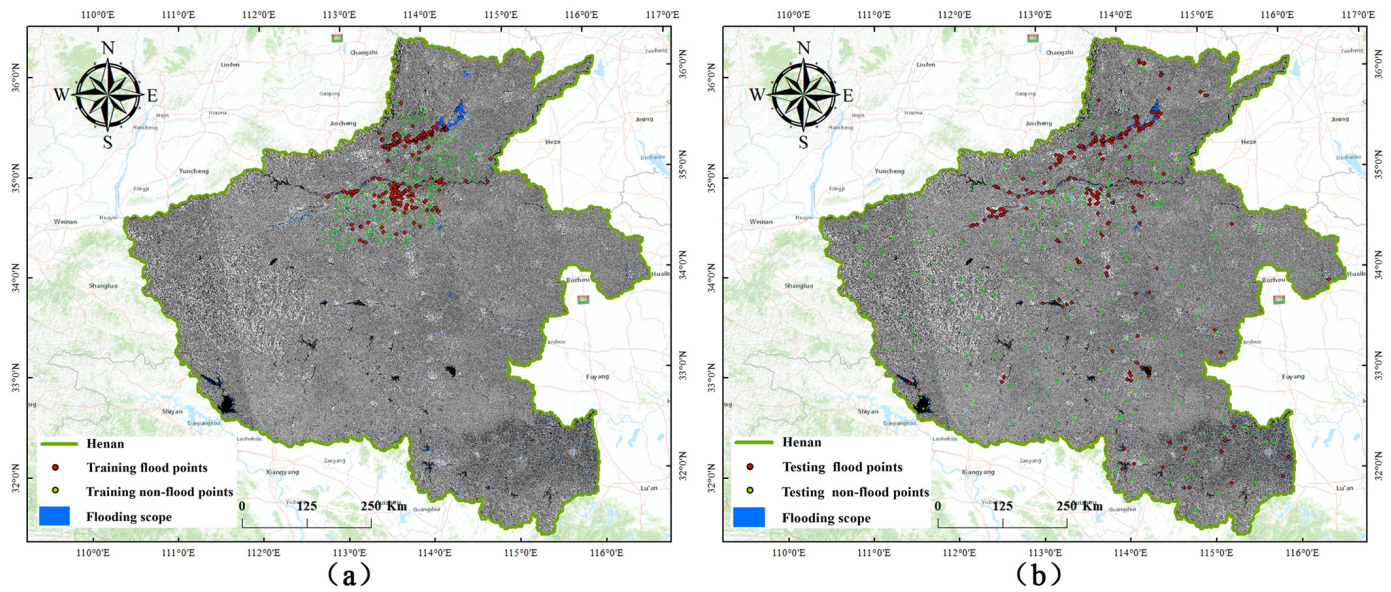


Figure 2. Distribution of flooding sample points: (a) training samples; (b) test and validation samples.

### 2.2.2. Flood Risk Assessment Indicator Data

Indicator factors were selected from three dimensions: hazard, exposure, and vulnerability, comprising a total of 21 as detailed in Table 1. Hazard indicators include rainfall, annual precipitation variability, land erosion modulus, elevation variation coefficient, topographic relief, slope, aspect, planar curvature, and profile curvature, summing up to nine. Exposure indicators are composed of the topographic wetness index (TWI), stream power index (SPI), flow accumulation (FA), NDVI, impervious area, and sediment transport index (STI), also totaling six. Vulnerability indicators include night lights, population density, Gross Domestic Product (GDP), medical facilities, educational level, and emergency shelters, also amounting to six.

Table 1. Source of indicator factors.

Raw Data	Indicator Factors	Abbreviation	Spatial Resolution	Time	Data Sources
DEM	Elevation variation coefficient	EVC	1000 × 1000 m	2000	National Science and Technology Infrastructure Platform—National Earth System Science Data Centre ( <a href="http://www.geodata.cn">http://www.geodata.cn</a> , accessed on 1 December 2023)
	Topographic relief	UR			
	Slope	Slope			
	Aspect	Aspect			
	Plane curvature	PC1			
	Profile curvature	PC2			
	Topographic wetness index	TWI			
	Stream power index	SPI			
	Flow accumulation	FA			
Sediment transport index	STI				
Annual precipitation in 2010–2020	Annual rainfall variability	ARV	1000 × 1000 m	2010–2020	National Science and Technology Infrastructure Platform—National Earth System Science Data Centre ( <a href="http://www.geodata.cn">http://www.geodata.cn</a> , accessed on 1 December 2023)

Table 1. Cont.

Raw Data	Indicator Factors	Abbreviation	Spatial Resolution	Time	Data Sources
Daily precipitation from 17–23 July 2021	Rainfall	Rainfall	11,132 × 11,132 m	2021	NASA Global Precipitation Measurement (GPM) v6 Precipitation Dataset ( <a href="https://gpm.nasa.gov/missions/GPM">https://gpm.nasa.gov/missions/GPM</a> , accessed on 1 December 2023)
Soil type	Land erosion modulus	LEM	1000 × 1000 m	1995	Resource Environmental Science and Data Centre ( <a href="https://www.resdc.cn/">https://www.resdc.cn/</a> , accessed on 1 February 2024)
NDVI	Normalized difference vegetation index	NDVI	30 × 30 m	2021	National Earth System Science Data Centre ( <a href="http://www.geodata.cn">http://www.geodata.cn</a> , accessed on 1 February 2024)
Impervious layer	Impervious area	IA	30 × 30 m	2020	Zenodo ( <a href="https://zenodo.org/record/5220816#.YrUCEPnrly">https://zenodo.org/record/5220816#.YrUCEPnrly</a> , accessed on 1 February 2024)
Population	Population density	POP	1000 × 1000 m	2020	ORNL ( <a href="https://landscan.ornl.gov">https://landscan.ornl.gov</a> , accessed on 1 February 2024)
Economy	Gross GDP	GDP	1000 × 1000 m	2020	GitHub ( <a href="https://github.com/thestarlab/ChinaGDP">https://github.com/thestarlab/ChinaGDP</a> , accessed on 1 February 2024)
POI	Emergency shelter	ES	1000 × 1000 m	2021	Golder Open Platform ( <a href="https://lbs.amap.com/">https://lbs.amap.com/</a> , accessed on 1 February 2024)
The Seventh Population Census	Medical facility	MF	1000 × 1000 m	2020	2020 China Census Information by County
Nighttime light data of DMSP-OLS	Educational level	EL	1000 × 1000 m	2020	Improved DMSP-OLS time series data for the China category by integrating DMSP-OLS and SNPP-VIIRS ( <a href="https://dataverse.harvard.edu/dataset.xhtml?persistentId=doi:10.7910/DVN/GIYGJU">https://dataverse.harvard.edu/dataset.xhtml?persistentId=doi:10.7910/DVN/GIYGJU</a> , accessed on 1 February 2024)

## (1) Hazard

A hazard indicates the potential damage from flooding within a certain period [38]. Heavy rainfall is a major influence on flooding, while topographic factors directly affect the flooding process [39]. Factors such as rainfall, variability in annual precipitation, and the land erosion rate directly impact the likelihood and severity of flooding events. Topographic elements, including the elevation variation coefficient, relief, slope, aspect, plane curvature, and profile curvature, influence flood runoff, flow direction, and velocity, increasing flood risk.

## (2) Exposure

Exposure refers to the likelihood of encountering floods over a specific period [33]. High TWI values signify a higher risk of waterlogging; higher SPI values indicate stronger stream power, which may exacerbate flooding; areas with high FA are more prone to flooding; NDVI reflects surface vegetation, with dense coverage mitigating flood risks; large impervious surfaces increase runoff and flood exposure; and high STI values may lead to channel obstruction and increase flood risk. Therefore, the topographic wetness index (TWI), stream power index (SPI), flow accumulation (FA), NDVI, impervious surfaces, and the sediment transport index (STI) are crucial in assessing regional flood exposure.

### (3) Vulnerability

Vulnerability refers to the overall capacity and manner in which a disaster-tolerant system reduces risk and damage [40]. Vulnerability factors encompass nighttime lighting, population density, GDP, presence of healthcare facilities, educational attainment, and emergency shelters. Among them, the level of urbanization and population density are derived from nighttime light intensity data. GDP quantifies the ability to cope with and recover from a disaster [41]. The presence of healthcare and educational facilities measures a region's resilience in the face of sudden flooding. In addition, the distribution and capacity of emergency shelters are critical to ensure the safety of people in the event of a disaster.

### 3. Risk Assessment Framework for Short-Term Rainstorm Urban Flood Disaster

Initially, key flood assessment factors are identified from the perspectives of a hazard, exposure, and vulnerability. Through a Pearson correlation analysis, multicollinearity among these factors is addressed, and the number of initial factors is reduced via dimensionality reduction. This process formed the basis for constructing a short-term rainstorm urban flood disaster risk assessment system. Subsequently, the WOA is employed to refine the weights, and models such as RF, SVM, and LR are integrated to develop the WRSL-Short-Term Flood Risk Assessment Model. Finally, the performance of the model is evaluated, and a flood risk assessment map is generated (Figure 3).

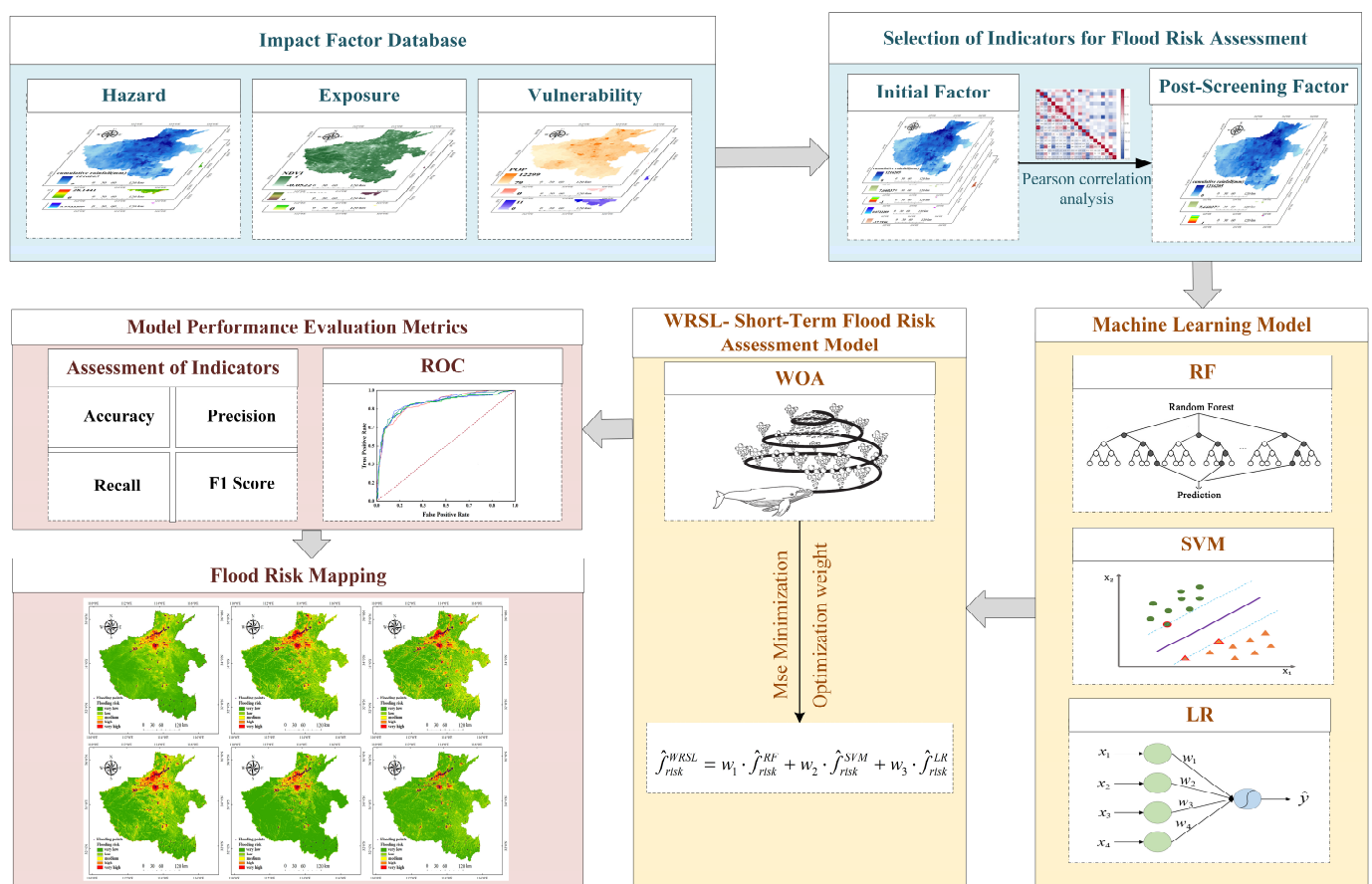


Figure 3. Research framework for risk assessment of short-term rainstorm urban flood disaster.

A framework for assessing the risk of short-term, storm-type urban flooding is developed from the three critical perspectives: hazard, exposure, and vulnerability (abbreviated as 'H-E-V'). The mathematical representation of this framework is detailed in Equation (1):

$$f_{risk}^{WRSL} = w_1 \cdot f_{risk}^{RF}(H, E, V) + w_2 \cdot f_{risk}^{SVM}(H, E, V) + w_3 \cdot f_{risk}^{LR}(H, E, V) \quad (1)$$

where  $f_{risk}^{WRSL}$  is the flood risk index of the WRSL-Short-Term Flood Risk Assessment Model;  $f_{risk}^{RF}(H, E, V)$ ,  $f_{risk}^{SVM}(H, E, V)$ , and  $f_{risk}^{LR}(H, E, V)$  are the flood risk indices from the RF, SVM, and LR models, respectively; and  $w_1$ ,  $w_2$ , and  $w_3$  denote the respective weights assigned to each model.

### 3.1. Integration Model Based on Whale Algorithm Optimization

The WRSL-Short-Term Flood Risk Assessment Model employs RF, SVM, and LR as baseline models, training them to obtain respective flood risk values and using three weighting factors ( $w_1$ ,  $w_2$ ,  $w_3$ ) to integrate the outputs of these models. In this study, the search is optimized with the mean square error (MSE) between the flood risk values assessed by the integrated model and the actual values. A smaller mean square error indicates a smaller error in the simulation results. Therefore, the mean square error is calculated as the value of the model fitness function to identify the best individual position. The mathematical expression of the objective function is as follows:

$$MSE = \frac{1}{n} \sum_{i=1}^n \left( f_i - \hat{f}_{risk}^{WRSL} \right)^2 \quad (2)$$

where  $n$  is the number of sample points; the  $f_i$  value of the training sample is 1 for flood points and 0 for non-flood points; and  $\hat{f}_{risk}^{WRSL}$  is the  $i$ -th integrated flood risk index.

WOA has the advantages of a minimal number of parameters and a robust optimization capability, and performs well in solving the minimization objective function problem [42]. Therefore, in this study, WOA is used to determine the numerical solutions of  $w_1$ ,  $w_2$  and  $w_3$  and optimize the weights of RF, SVM, and LR models to obtain the optimal combination of flood risk values.

(1) The mathematical model of WOA consists of three main components: encircling prey, spiral bubble hunting, and random search for prey. The first part involves encircling prey. Humpback whales initially pinpoint the location of the prey and progressively encircle it by adjusting their position. During this process, the search agent nearest to the target becomes the optimal position, and other whales update their positions gradually to encircle the prey effectively. The position update calculation is expressed as follows:

$$D_{iter} = |CX * (t_{iter}) - X(t_{iter})| \quad (3)$$

$$X(t_{iter} + 1) = X * (t_{iter}) - A \cdot D_{iter} \quad (4)$$

where  $D_{iter}$  is the distance between the current position and the optimal position;  $X * (t_{iter})$  is the position vector of the optimally fit whale;  $X(t_{iter})$  is the current individual's position vector;  $t_{iter}$  represents the current iteration; and  $A$  and  $C$  are parameter vectors defined by

$$A = a \cdot (2r_1 - 1) \quad (5)$$

$$C = 2r_2 \quad (6)$$

where  $r_1$  and  $r_2$  are random vectors between 0 and 1; a decrease linearly from 2 to 0 over the iterations is as shown below:

$$a = 2 \cdot \left( 1 - \frac{t_{iter}}{t_{max\_iter}} \right) \quad (7)$$

where  $t_{max\_iter}$  is the maximum number of iterations.

The second part is a spiral bubble Hunting. As whales encircle prey, they may choose to tighten the circle or advance in a spiral motion. Assuming that whales have  $P_i$  probability of choosing to shrink the encirclement and  $1 - P_i$  probability of choosing to spiral forward,

respectively, during a spiral bubble hunt, the mathematical model expression for this simultaneous choice is as follows:

$$X(t_{iter} + 1) = \begin{cases} X * (t_{iter}) - A \cdot D_{iter}, & P < P \\ X * (t_{iter}) + D' e^{bl} \cos(2\pi l), & P \geq P \end{cases} \quad (8)$$

where  $P$  is a random number between 0 and 1;  $l \subseteq (-1, 1)$ ;  $D' = |X(t_{iter}) - X * (t_{iter})|$  is the distance between each current individual and the optimal individual;  $b$  is a constant to describe the spiral shape; and  $P_i$  is generally taken as 0.5.

From Equation (7), it can be seen that as the number of iterations increases,  $a$  decreases linearly, while at the same time the value of each element in  $A$  fluctuates between  $[-a, a]$ ; when  $[-a, a]$ , the next position of the individual whale is any position between the current position of the individual whale and the prey. The algorithm sets that when the absolute value of each element value in  $A$  is less than 1, the whale will launch a strike at the prey.

The third part is a random search for prey. The search mechanism for each whale depends on the values in  $A$ . If the absolute values are less than 1, the whale updates its position based on the optimal position and conducts a local search. If greater than 1, it forces the whale away from the optimal position, and updates occur based on a randomly selected whale's position, triggering a global search. The mathematical models for these actions are

$$D_{rand} = |C \cdot X_{rand}(t_{iter}) - X(t_{iter})| \quad (9)$$

$$X(t_{iter} + 1) = X_{rand}(t_{iter}) - A \cdot D_{rand} \quad (10)$$

where  $X_{rand}$  is the position vector of a randomly selected individual whale, and  $D_{rand}$  is the distance to the prey.

In the experimentally designed WOA, each whale's position represents potential weight values for the models RF, SVM, and LR. When the algorithm runs, the position of the optimal solution indicates the combination of weights that minimizes the mean square error of the integrated model, thereby determining the most effective model weights.

#### (2) RF

RF employs a bootstrap sampling technique to train numerous decision trees and aggregates them into a model [43]. This method improves the model's stability and generalization ability by aggregating outputs of the trees through voting or weighted averaging [44]. It is effective for both classification and regression tasks. The construction process of a RF involves (1) using the bootstrap method to randomly generate  $K$  subsets from the entire dataset and constructing  $K$  classification trees; (2) selecting several features randomly at any tree node and choosing the best one for splitting; (3) continuing to split each tree until all training samples at a node fall into the same category; (4) combining all the trees to form the complete RF.

#### (3) SVM

The SVM is a machine learning algorithm based on VC dimension theory and the principle of structural risk minimization within statistical learning theory [45], demonstrating significant advantages in addressing small samples, non-linearities [46,47], and high-dimensional pattern recognition [48]. Originally developed for binary classification, the fundamental concept of SVMs involves identifying an optimal classification hyperplane that maximizes the margin between the nearest data points of two classes [49]. The data points that define this margin are known as support vectors, and the hyperplane runs centrally through the maximized margin. In cases where data are not linearly separable, the model uses a kernel function to map data points to a higher dimensional space, making linear separation possible. Misclassified points are given reduced weight to minimize their influence on the model [50].

#### (4) LR

A LR model is a generalized linear model [51] that establishes a multiple-regression relationship between a dependent variable and several independent variables to predict

the probability of an event's occurrence in a specific area [25]. The dependent variable in LR is categorical; specifically, the occurrence of flooding is modeled. A value of '1' indicates flooding, while '0' indicates no flooding.

LR predicts the probability of flood events by expressing the logarithmic odds of flooding as a linear combination of multiple independent variables, as detailed in Mathematical Expression (12):

$$\log \text{it}(f_{risk}^{LR}) = \beta_0 + \beta_1 x_1 + \dots + \beta_n x_n \quad (11)$$

$$f_{risk}^{LR} = \frac{e^{\beta_0 + \beta_1 x_1 + \dots + \beta_n x_n}}{1 + e^{\beta_0 + \beta_1 x_1 + \dots + \beta_n x_n}} \quad (12)$$

where  $\log \text{it}(f_{risk}^{LR})$  is the log odds of a flood event occurring;  $\beta_0, \beta_1, \beta_2, \dots, \beta_n$  is the LR coefficient; and  $x_0, x_1, x_2, \dots, x_n$  is the impact factor.

### 3.2. Pearson's Correlation Coefficient

The Pearson correlation analysis method measures the correlation between two variables, ensuring that the indicator factors used in model training maintain a high degree of independence. This analysis supports the construction and optimization of subsequent machine learning models. The mathematical expression of the Pearson correlation coefficient is provided in Equation (13).

$$r = \sigma_{xy}^2 / \sigma_x \sigma_y \quad (13)$$

where  $r$  represents the correlation coefficient;  $\sigma_{xy}^2$  is the covariance between variables  $x$  and  $y$ ;  $\sigma_x$  is the standard deviation of variable  $x$ ; and  $\sigma_y$  is the standard deviation of variable  $y$ . The value of  $r$  ranges from  $-1$  to  $1$ , indicating the correlation direction; a negative  $r$  signifies a negative correlation, whereas a positive  $r$  indicates a positive correlation. The closer  $|r|$  is to  $1$ , the stronger the correlation between the variables.

### 3.3. Precision Analysis Evaluation Indicators

To objectively assess the performance of different models, the experiment uses the accuracy, Precision, Recall, F1 Score, and Receiver Operating Characteristic Curve (ROC) for evaluation.  $TP$  denotes the number of true positives,  $TN$  denotes the number of true negatives,  $FP$  denotes the number of false positives, and  $FN$  denotes the number of false negatives.

Accuracy is defined as the ratio of correctly classified samples to the total number of samples, serving as a comprehensive statistical measure. This is expressed mathematically in Formula (14):

$$\text{Accuracy} = \frac{TP + TN}{TP + TN + FP + FN} \quad (14)$$

Precision, also termed as positive predictive value, measures the ratio of correctly identified positive samples to the total samples classified as positive by the model. It focuses on the accuracy of positively identified data and is defined in Formula (15):

$$\text{Precision} = \frac{TP}{TP + FP} \quad (15)$$

Recall, or sensitivity, indicates the ratio of correctly identified positive samples to the actual positive samples. This metric concentrates on the accuracy of truly positive identifications and is expressed in Formula (16):

$$\text{Recall} = \frac{TP}{TP + FN} \quad (16)$$

The F1 Score, a harmonic mean of Precision and Recall, balances both metrics and is a standard statistical measure for classification accuracy. The score ranges between 0 and 1, with higher values indicating superior model performance, as shown in Equation (17).

$$F_1 = 2 \times \frac{Precision \times Recall}{Precision + Recall} \tag{17}$$

The ROC curve illustrates the relationship between model predictions and actual outcomes [52]. The curve plots the False Positive Rate (FPR) against the True Positive Rate (TPR), and by varying the classification threshold, it describes the model’s generalization capability. The area beneath the ROC curve, known as the AUC value, quantifies the accuracy; a larger AUC value signifies a more accurate model [53].

#### 4. Experimental Analysis and Results

##### 4.1. Correlation Analysis of Indicators for Risk Assessment of Short-Term Heavy Rainfall-Based Urban Floods

The study utilized Pearson correlation analysis to mitigate potential collinearity among factors, thereby preserving the model’s efficiency and accuracy. Results from the Pearson correlation (Figure 4), revealed significant correlations—all exceeding 0.6—among profile curvature, topographic relief, STI, medical facilities, and night lights. Consequently, these five indicator factors were excluded to refine the indicator system (Figure 5).

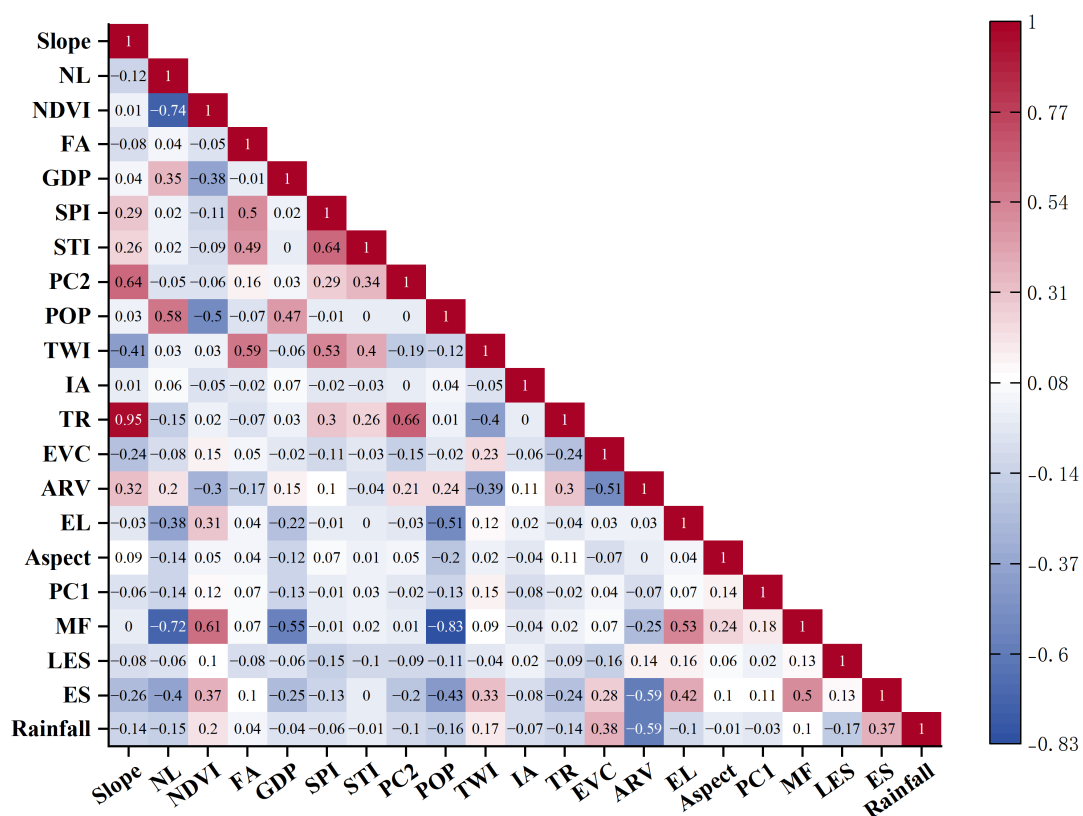
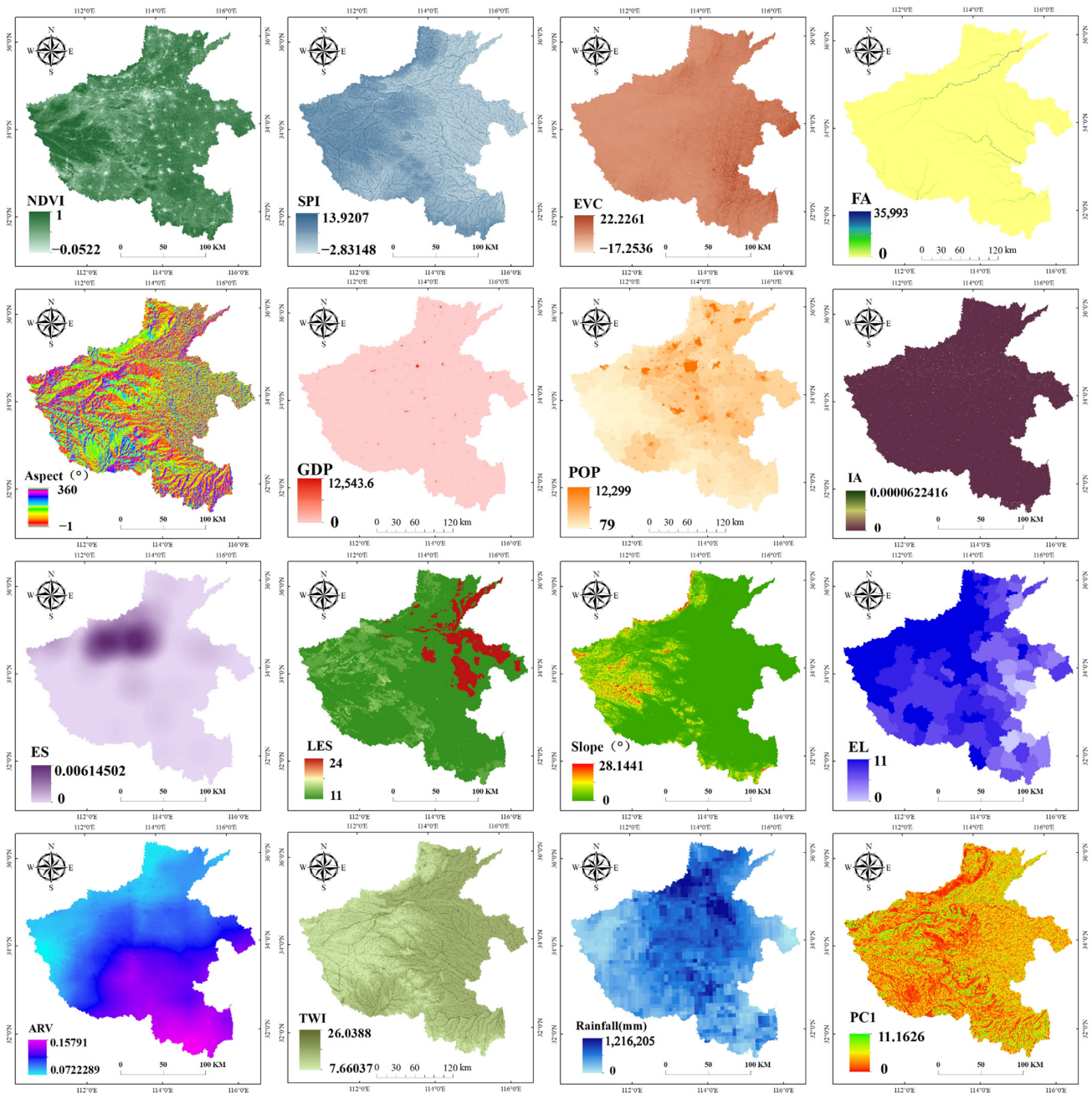


Figure 4. Pearson correlation analysis results.

##### 4.2. Model Performance Assessment

In the WOA, optimal settings for population size (Pop) and maximum iterations are crucial for algorithm performance. A small Pop size risks entrapment in local optima, while a large Pop size may increase computational demands and hinders convergence. Similarly, too few iterations result in insufficient search depth, whereas too many prolong computation time and decrease convergence rates [54]. The experiment settings included

a Pop of 30 and a maximum of 100 iterations. To enhance stability and robustness, the WOA was performed 10 times, demonstrating convergence in the results; thus, the optimal outcome was selected as the final model output. Figure 6 illustrates the fitness curves, showing the algorithm's gradual convergence towards the optimal solution, achieved after 43 total iterations.



**Figure 5.** Indicator system for flood risk assessment.

The ROC curves compare the performance of the WRSL-Short-Term Flood Risk Assessment Model with that of the average weight RF-SVM-LR model, as well as the RF, SVM, LR, and XGB models, as shown in Figure 6. The accuracy, Precision, Recall, F1 Score, and AUC for these models are detailed in Table 2.

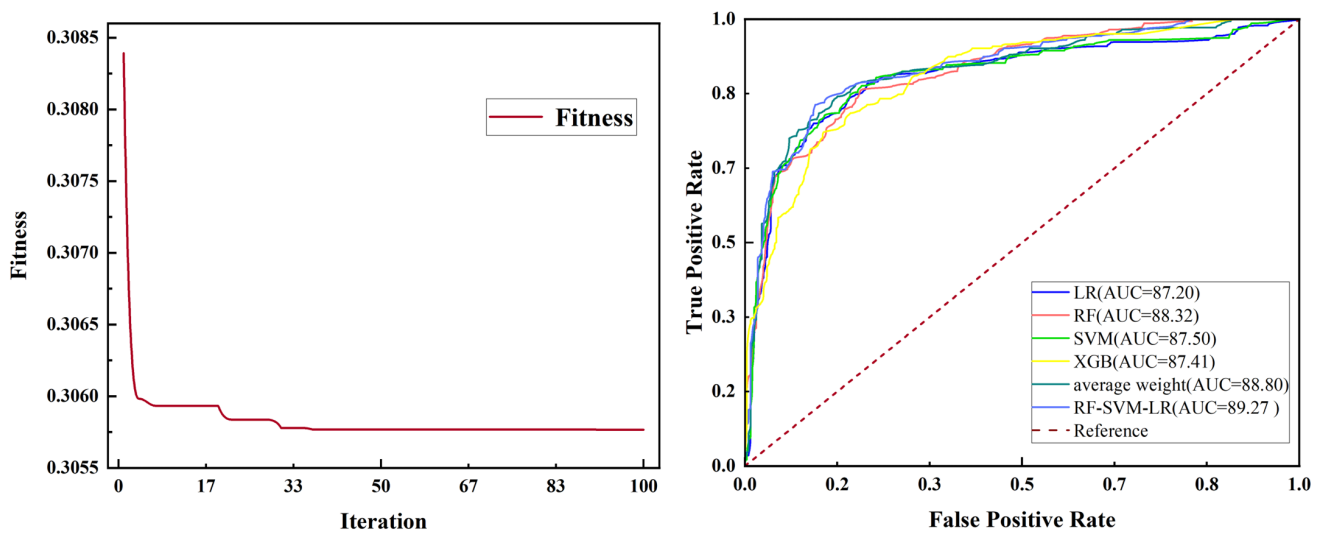


Figure 6. Fitness curves vs. ROC curves for all models.

Table 2. Model performance evaluation results.

Name	Accuracy (%)	Precision (%)	Recall (%)	F1 Score (%)	AUC (%)
RF	80.74	81.77	69.16	74.94	88.32
SVM	82.88	83.87	72.90	78.00	87.50
LR	82.49	84.83	70.56	77.04	87.20
XGBoost	78.40	81.99	61.68	70.4	87.41
average weight RF-SVM-LR	83.85	86.59	72.43	78.88	88.80
WRS�-Short-Term Flood Risk Assessment Model	84.24	79.82	83.18	81.46	89.27

According to the accuracy results, the WRS�-Short-Term Flood Risk Assessment Model outperforms RF, SVM, LR, XGBoost, and average weight-RF-SVM-LR in assessing flood risk, exhibiting superior performance in terms of accuracy, recall, F1 score, and AUC, though it shows weaker precision metrics.

The increase in accuracy signifies that the model more accurately predicts both flood and non-flood points. Recall demonstrates the model's enhanced capability to identify actual flood hazards, effectively reducing false alarms. The F1 score, a balanced average of precision and recall, serves as a comprehensive metric for evaluating the model's performance. The increase in F1 Score reflects the model's improved balance between avoiding false alarms and reducing underreporting. Similarly, the rise in AUC demonstrates the model's enhanced ability to distinguish between flood and non-flood points. Despite a decrease in precision—about 5% lower compared to other models, due to misclassifying a small number of non-flooded points as high-risk areas—the significant boost in recall more than compensates for this shortfall, resulting in enhanced overall model performance. This shows that the WRS�-Short-Term Flood Risk Assessment Model does not unduly sacrifice precision while prioritizing recall, thereby providing a more comprehensive and accurate assessment of flood risk.

#### 4.3. Mapping of Flood Risk Assessment Results

Using the natural breakpoint method, flood risk assessment results are categorized into five levels, very-high-risk, high-risk, medium-risk, low-risk, and very-low-risk areas, as shown in Figure 7. The flood risk map produced by the optimal model, the WRS�-Short-Term Flood Risk Assessment Model, shows that the very-high- and high-risk zones predominantly occur in areas characterized by low terrain, gentle slopes, high rainfall, sparse vegetation cover, and high terrain humidity. The cities of Zhengzhou, Jiaozuo, and Xinxiang are the most significantly impacted, with Hebei, Luoyang, Kaifeng, and Anyang

also being affected to a lesser extent. Rapid urbanization and population growth have transformed large expanses of natural land into residential and commercial zones, diminishing areas that naturally regulate water, such as wetlands and grasslands. These areas were initially capable of absorbing and storing significant volumes of rainwater; however, due to the proliferation of impervious surfaces such as concrete and asphalt, rainwater fails to infiltrate, leading to rapid pooling and increased surface runoff, thus exacerbating flooding risks. In addition, the flat topography and minimal elevation changes in these regions hinder the swift drainage of rainwater, causing water accumulation and elevated flood risks. Medium risk areas, influenced by topography, are dispersed throughout the province, prone to rainwater accumulation. Low-risk and very-low-risk areas are typically situated at higher elevations, characterized by dense vegetation and low population densities. In these regions, the higher elevation facilitates quicker water flow, reducing the time for water accumulation. Dense vegetation enhances rainwater absorption and decreases surface runoff. Low population density minimizes land development pressure, preserving natural hydrological regulation zones. Additionally, a low level of economic activity helps maintain the natural hydrological cycle by limiting land and infrastructure development.

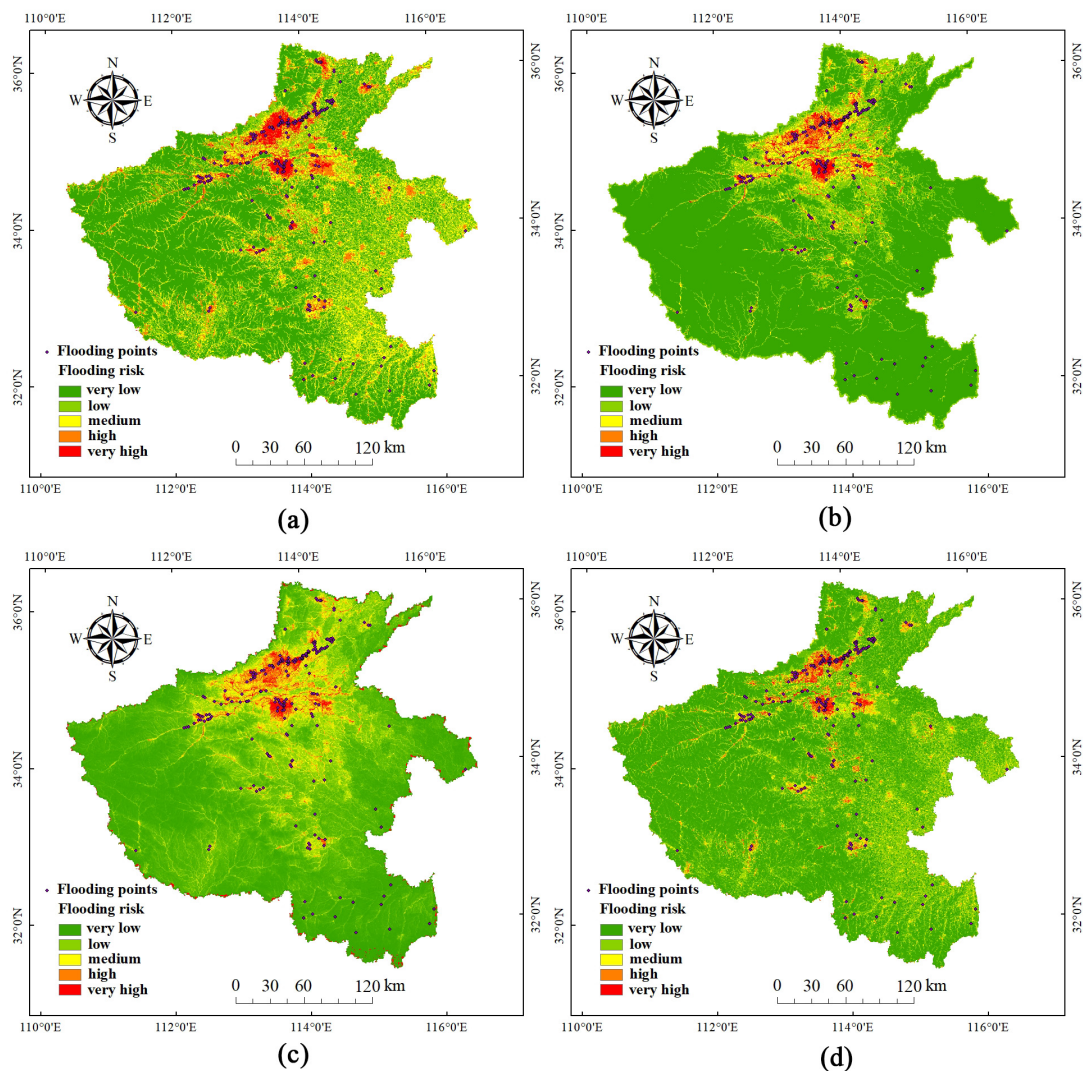
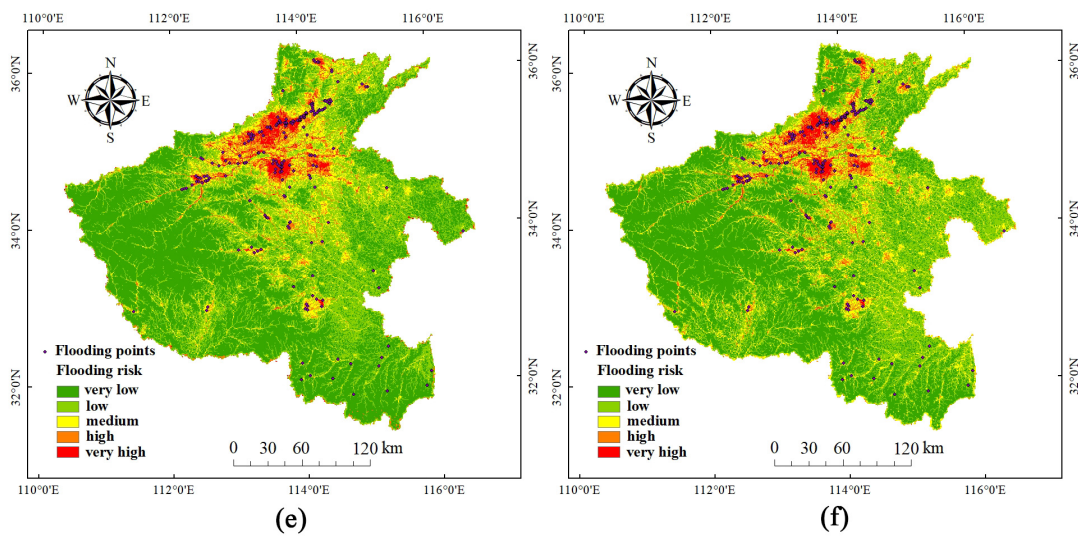
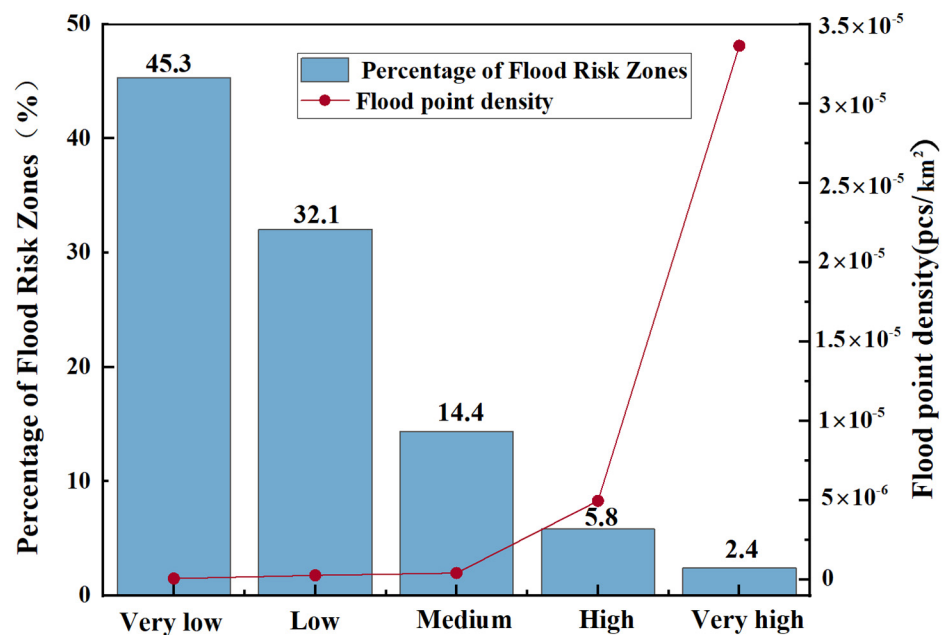


Figure 7. Cont.



**Figure 7.** Flood risk maps generated by the different models: (a) RF, (b) SVM, (c) LR, (d) XGBoost, (e) average weight RF-SVM-LR, and (f) WRSL-Short-Term Flood Risk Assessment Model.

The flood risk zoning results and flood point densities derived from the WRSL-Short-Term Flood Risk Assessment Model are presented in Figure 8. The distribution of risk zones is as follows, an extremely-low-risk area (45.3%), low-risk area (32.1%), medium-risk area (14.4%), high-risk area (5.8%), and extremely-high-risk area (2.4%), each associated with respective flood point densities, corresponding to flood point densities of  $7.99 \times 10^{-8}$ ,  $2.82 \times 10^{-7}$ ,  $4.21 \times 10^{-7}$ ,  $4.79 \times 10^{-7}$ , and  $3.36 \times 10^{-5}$  Pcs/km<sup>2</sup>. Most of the study area is classified into extremely-low-risk and low-risk categories. As risk levels increase, there is a corresponding rise in the density of flood points, demonstrating that the risk area categorization of the WRSL model aligns with the actual distribution of flood points in the region.



**Figure 8.** WRSL-Short-Term Flood Risk Assessment Model: flood risk zoning and flood point density statistics.

## 5. Discussion

Experiments confirmed the reliability of the short-term storm-type urban flood risk assessment model proposed in this study. Traditional integration methods such as Bagging, Boosting, Random Subspace (RS), Stacking, and Blending faced challenges with overfitting and parameter tuning. In contrast, the WOA performed an efficient global search, automatically adjusted its search strategy, and adapted to varying environments, proving more robust to outliers [54]. Therefore, WOA can address the limitations of the aforementioned integration methods, enhancing the model's performance and robustness. The WRSL-Short-Term Flood Risk Assessment Model outperforms single models in terms of accuracy, recall, F1 score, and AUC, mainly because it synergizes the strengths of RF, SVM, and LR [55–57]. This integration reduces the bias and variance inherent in single models, thus enabling more reliable predictions. RF is particularly robust in handling nonlinear and complex relationships, especially with high-dimensional data, by integrating multiple decision trees to minimize overfitting. SVM excels in small sample and high-dimensional data scenarios, adapting to different data structures via kernel functions. LR is valued for the interpretability of its models and suits classification problems, particularly binary classifications, offering clear predictions and straightforward models.

This study illustrates the benefits of an integrated learning approach for short-term heavy rainfall-based urban flood risk assessment, highlighting its effectiveness in enhancing the accuracy and robustness of assessments. The flood risk assessment results indicate higher risks in the central, eastern, and northeastern parts of Henan Province, providing crucial guidance for resource allocation and emergency management. In practice, government and emergency management authorities can use these results to prioritize resource distribution, ensuring that critical areas receive necessary support. While this study focuses on integrating three machine learning models—RF, SVM, and LR—future research could explore combinations of other models like XGBoost, Artificial Neural Network, Decision Tree, and K-Nearest Neighbor to further enhance performance. Additionally, comparative studies with other integration methods such as Bagging, Boosting, RS, Stacking, and Blending will be included in future experiments to deeply investigate the differences between the WRSL-Short-Term Flood Risk Assessment Model and alternative approaches.

## 6. Conclusions

In this study, the flooding disaster resulting from short-term extreme rainstorms in Henan Province from 17 to 23 July 2021 serves as a case example. Influencing factors were selected from three perspectives: hazard, exposure, and vulnerability. Pearson correlation analysis was employed to reduce the multiple covariance among these factors. To harness the strengths of RF, SVM, and LR models, an integrated learning model was developed, utilizing the WOA as an optimization method to determine the optimal weights of the model. This approach aimed to minimize the discrepancy between the flood risk assessment and the actual disaster outcomes. Ultimately, an urban flood risk assessment map was produced. The specific conclusions are as follows:

(1) The WRSL-Short-Term Flood Risk Assessment Model developed in this study outperforms both the single model and the average weight RF-SVM-LR model in terms of accuracy, Recall, F1 Score, and AUC. It offers a more precise assessment of flood risk and presents a novel approach to evaluating the risks associated with short-term rainstorms, enabling a more accurate assessment of the risk to the affected area.

(2) The optimally performing WRSL-Short-Term Flood Risk Assessment Model was applied to evaluate flood risk from short-term heavy rainfall in Henan Province. The risks were stratified into five categories, a very-low-risk zone, low-risk zone, medium-risk zone, high-risk zone, and very-high-risk zone, constituting 45.3%, 32.1%, 14.4%, 5.8%, and 2.4% of the area, respectively. The analysis indicates that the very-high-risk and high-risk zones predominantly occur in the central, eastern, and northeastern regions of Henan Province, largely in low-lying, heavily urbanized areas such as Zhengzhou, Jiaozuo, and Xinxiang.

**Author Contributions:** X.W. proposed the methodology and wrote the manuscript. H.Z. and L.H. assisted in refining the study methodology, with H.Z. serving as a corresponding author. J.M. and F.S. collected the data. All authors have read and agreed to the published version of the manuscript.

**Funding:** This research was funded by Science and Technology Innovation Program for Postgraduate students in IDP subsidized by Fundamental Research Funds for the Central Universities (Grant No. ZY20240303).

**Institutional Review Board Statement:** Not applicable.

**Informed Consent Statement:** Not applicable.

**Data Availability Statement:** Dataset available on request from the authors.

**Conflicts of Interest:** The authors declare no conflicts of interest.

## References

- Zhang, W.; Villarini, G.; Vecchi, G.A.; Smith, J.A. Urbanization exacerbated the rainfall and flooding caused by hurricane Harvey in Houston. *Nature* **2018**, *563*, 384–388. [[CrossRef](#)]
- Zeľeňáková, M.; Fijko, R.; Labant, S.; Weiss, E.; Markovič, G.; Weiss, R. Flood risk modelling of the Slatvinec stream in Kružlov village, Slovakia. *J. Clean. Prod.* **2019**, *212*, 109–118. [[CrossRef](#)]
- Bubeck, P.; Thieken, A.H. What helps people recover from floods? Insights from a survey among flood-affected residents in Germany. *Reg. Environ. Chang.* **2018**, *18*, 287–296. [[CrossRef](#)]
- Ward, P.J.; Jongman, B.; Aerts, J.C.J.H.; Bates, P.D.; Botzen, W.J.W.; Diaz Loaiza, A.; Hallegatte, S.; Kind, J.M.; Kwadijk, J.; Scussolini, P.; et al. A global framework for future costs and benefits of river-flood protection in urban areas. *Nat. Clim. Chang.* **2017**, *7*, 642–646. [[CrossRef](#)]
- Re, S. *Mind the Risk: A Global Ranking of Cities under Threat from Natural Disasters*; Swiss Re: Zürich, Switzerland, 2013.
- Kundzewicz, Z.W.; Kanae, S.; Seneviratne, S.I.; Handmer, J.; Nicholls, N.; Peduzzi, P.; Mechler, R.; Bouwer, L.M.; Arnell, N.; Mach, K. Flood risk and climate change: Global and regional perspectives. *Hydrol. Sci. J.* **2014**, *59*, 1–28. [[CrossRef](#)]
- Costache, R.; Zaharia, L. Flash-flood potential assessment and mapping by integrating the weights-of-evidence and frequency ratio statistical methods in GIS environment—case study: Bâsca Chiojdului River catchment (Romania). *J. Earth Syst. Sci.* **2017**, *126*, 59. [[CrossRef](#)]
- Li, C.; Sun, N.; Lu, Y.; Guo, B.; Wang, Y.; Sun, X.; Yao, Y. Review on urban flood risk assessment. *Sustainability* **2023**, *15*, 765. [[CrossRef](#)]
- Benito, G.; Lang, M.; Barriendos, M.; Llasat, M.C.; Francés, F.; Ouarda, T.; Thorndycraft, V.; Enzel, Y.; Bardossy, A.; Coeur, D. Use of systematic, palaeoflood and historical data for the improvement of flood risk estimation. Review of scientific methods. *Nat. Hazards* **2004**, *31*, 623–643.
- Werritty, A.; Paine, J.; Macdonald, N.; Rowan, J.; McEwen, L. Use of multi-proxy flood records to improve estimates of flood risk: Lower River Tay, Scotland. *Catena* **2006**, *66*, 107–119. [[CrossRef](#)]
- Liu, Z.; Merwade, V. Separation and prioritization of uncertainty sources in a raster based flood inundation model using hierarchical Bayesian model averaging. *J. Hydrol.* **2019**, *578*, 124100. [[CrossRef](#)]
- Zhao, G.; Pang, B.; Xu, Z.; Peng, D.; Xu, L. Assessment of urban flood susceptibility using semi-supervised machine learning model. *Sci. Total Environ.* **2019**, *659*, 940–949. [[CrossRef](#)]
- Chowdary, V.; Chandran, R.V.; Neeti, N.; Bothale, R.; Srivastava, Y.; Ingle, P.; Ramakrishnan, D.; Dutta, D.; Jeyaram, A.; Sharma, J. Assessment of surface and sub-surface waterlogged areas in irrigation command areas of Bihar state using remote sensing and GIS. *Agric. Water Manag.* **2008**, *95*, 754–766. [[CrossRef](#)]
- Meraner, A.; Ebel, P.; Zhu, X.X.; Schmitt, M. Cloud removal in Sentinel-2 imagery using a deep residual neural network and SAR-optical data fusion. *ISPRS J. Photogramm. Remote Sens.* **2020**, *166*, 333–346. [[CrossRef](#)]
- Xu, G. A Review of Remote Sensing of Atmospheric Profiles and Cloud Properties by Ground-Based Microwave Radiometers in Central China. *Remote Sens.* **2024**, *16*, 966. [[CrossRef](#)]
- Roy, S.; Bose, A.; Chowdhury, I.R. Flood risk assessment using geospatial data and multi-criteria decision approach: A study from historically active flood-prone region of Himalayan foothill, India. *Arab. J. Geosci.* **2021**, *14*, 999. [[CrossRef](#)]
- Wijayarathne, D.B.; Coulibaly, P. Identification of hydrological models for operational flood forecasting in St. John's, Newfoundland, Canada. *J. Hydrol. Reg. Stud.* **2020**, *27*, 100646. [[CrossRef](#)]
- Dutta, D.; Herath, S.; Musiaka, K. A mathematical model for flood loss estimation. *J. Hydrol.* **2003**, *277*, 24–49. [[CrossRef](#)]
- Aziz, K.; Rahman, A.; Fang, G.; Shrestha, S. Application of artificial neural networks in regional flood frequency analysis: A case study for Australia. *Stoch. Environ. Res. Risk Assess.* **2014**, *28*, 541–554. [[CrossRef](#)]
- Mekanik, F.; Imteaz, M.; Gato-Trinidad, S.; Elmahdi, A. Multiple regression and Artificial Neural Network for long-term rainfall forecasting using large scale climate modes. *J. Hydrol.* **2013**, *503*, 11–21. [[CrossRef](#)]
- Xu, Z.; Li, J. Short-term inflow forecasting using an artificial neural network model. *Hydrol. Process.* **2002**, *16*, 2423–2439. [[CrossRef](#)]

22. Zhu, H.; Leandro, J.; Lin, Q. Optimization of artificial neural network (ANN) for maximum flood inundation forecasts. *Water* **2021**, *13*, 2252. [[CrossRef](#)]
23. Tehrany, M.S.; Pradhan, B.; Mansor, S.; Ahmad, N. Flood susceptibility assessment using GIS-based support vector machine model with different kernel types. *Catena* **2015**, *125*, 91–101. [[CrossRef](#)]
24. Wang, Z.; Lai, C.; Chen, X.; Yang, B.; Zhao, S.; Bai, X. Flood hazard risk assessment model based on random forest. *J. Hydrol.* **2015**, *527*, 1130–1141. [[CrossRef](#)]
25. Al-Juaidi, A.E.; Nassar, A.M.; Al-Juaidi, O.E. Evaluation of flood susceptibility mapping using logistic regression and GIS conditioning factors. *Arab. J. Geosci.* **2018**, *11*, 765. [[CrossRef](#)]
26. Ma, M.; Zhao, G.; He, B.; Li, Q.; Dong, H.; Wang, S.; Wang, Z. XGBoost-based method for flash flood risk assessment. *J. Hydrol.* **2021**, *598*, 126382. [[CrossRef](#)]
27. Ying, X. An overview of overfitting and its solutions. *J. Phys. Conf. Ser.* **2019**, *1168*, 022022. [[CrossRef](#)]
28. Raschka, S. Model evaluation, model selection, and algorithm selection in machine learning. *arXiv* **2018**, arXiv:1811.12808.
29. Yao, J.; Zhang, X.; Luo, W.; Liu, C.; Ren, L. Applications of Stacking/Blending ensemble learning approaches for evaluating flash flood susceptibility. *Int. J. Appl. Earth Obs. Geoinf.* **2022**, *112*, 102932. [[CrossRef](#)]
30. Chapi, K.; Singh, V.P.; Shirzadi, A.; Shahabi, H.; Bui, D.T.; Pham, B.T.; Khosravi, K. A novel hybrid artificial intelligence approach for flood susceptibility assessment. *Environ. Model. Softw.* **2017**, *95*, 229–245. [[CrossRef](#)]
31. Chen, J.; Huang, G.; Chen, W. Towards better flood risk management: Assessing flood risk and investigating the potential mechanism based on machine learning models. *J. Environ. Manag.* **2021**, *293*, 112810. [[CrossRef](#)]
32. Pham, B.T.; Phong, T.V.; Nguyen-Thoi, T.; Parial, K.; Singh, S.K.; Ly, H.-B.; Nguyen, K.T.; Ho, L.S.; Le, H.V.; Prakash, I. Ensemble modeling of landslide susceptibility using random subspace learner and different decision tree classifiers. *Geocarto Int.* **2022**, *37*, 735–757. [[CrossRef](#)]
33. Islam, A.R.M.T.; Talukdar, S.; Mahato, S.; Kundu, S.; Eibek, K.U.; Pham, Q.B.; Kuriqi, A.; Linh, N.T.T. Flood susceptibility modelling using advanced ensemble machine learning models. *Geosci. Front.* **2021**, *12*, 101075. [[CrossRef](#)]
34. Arabameri, A.; Saha, S.; Chen, W.; Roy, J.; Pradhan, B.; Bui, D.T. Flash flood susceptibility modelling using functional tree and hybrid ensemble techniques. *J. Hydrol.* **2020**, *587*, 125007. [[CrossRef](#)]
35. Li, X.; Lu, H.; Zhang, Z.; Xing, W. Spatio-temporal variations of the major meteorological disasters and its response to climate change in Henan Province during the past two millennia. *PeerJ* **2021**, *9*, e12365. [[CrossRef](#)]
36. Sun, J.; Fu, S.; Wang, H.; Zhang, Y.; Chen, Y.; Su, A.; Wang, Y.; Tang, H.; Ma, R. Primary characteristics of the extreme heavy rainfall event over Henan in July 2021. *Atmos. Sci. Lett.* **2023**, *24*, e1131. [[CrossRef](#)]
37. Zhu, H.; Yao, J.; Meng, J.; Cui, C.; Wang, M.; Yang, R. A Method to Construct an Environmental Vulnerability Model Based on Multi-Source Data to Evaluate the Hazard of Short-Term Precipitation-Induced Flooding. *Remote Sens.* **2023**, *15*, 1609. [[CrossRef](#)]
38. Parmesan, C.; Morecroft, M.D.; Trisurat, Y. *Climate Change 2022: Impacts, Adaptation and Vulnerability*; Cambridge University Press: Cambridge, UK, 2022.
39. Zhang, P.; Sun, W.; Xiao, P.; Yao, W.; Liu, G. Driving factors of heavy rainfall causing flash floods in the middle reaches of the Yellow River: A case study in the Wuding River Basin, China. *Sustainability* **2022**, *14*, 8004. [[CrossRef](#)]
40. Yang, Y.; Guo, H.; Wang, D.; Ke, X.; Li, S.; Huang, S. Flood vulnerability and resilience assessment in China based on super-efficiency DEA and SBM-DEA methods. *J. Hydrol.* **2021**, *600*, 126470. [[CrossRef](#)]
41. Zhao, H.; Gu, T.; Tang, J.; Gong, Z.; Zhao, P. Urban flood risk differentiation under land use scenario simulation. *iScience* **2023**, *26*, 106479. [[CrossRef](#)]
42. Mirjalili, S.; Lewis, A. The whale optimization algorithm. *Adv. Eng. Softw.* **2016**, *95*, 51–67. [[CrossRef](#)]
43. Breiman, L. Random forests. *Mach. Learn.* **2001**, *45*, 5–32. [[CrossRef](#)]
44. Fawagreh, K.; Gaber, M.M.; Elyan, E. Random forests: From early developments to recent advancements. *Syst. Sci. Control. Eng. Open Access J.* **2014**, *2*, 602–609. [[CrossRef](#)]
45. Cortes, C.; Vapnik, V. Support-vector networks. *Mach. Learn.* **1995**, *20*, 273–297. [[CrossRef](#)]
46. Lee, S.; Hong, S.-M.; Jung, H.-S. A Support Vector Machine for Landslide Susceptibility Mapping in Gangwon Province, Korea. *Sustainability* **2017**, *9*, 48. [[CrossRef](#)]
47. Ballabio, C.; Sterlacchini, S. Support vector machines for landslide susceptibility mapping: The Staffora River Basin case study, Italy. *Math. Geosci.* **2012**, *44*, 47–70. [[CrossRef](#)]
48. Liu, X.; Gao, C.; Li, P. A comparative analysis of support vector machines and extreme learning machines. *Neural Netw.* **2012**, *33*, 58–66. [[CrossRef](#)] [[PubMed](#)]
49. Marjanović, M.; Kovačević, M.; Bajat, B.; Voženilek, V. Landslide susceptibility assessment using SVM machine learning algorithm. *Eng. Geol.* **2011**, *123*, 225–234. [[CrossRef](#)]
50. Jebur, M.N.; Pradhan, B.; Tehrany, M.S. Manifestation of LiDAR-derived parameters in the spatial prediction of landslides using novel ensemble evidential belief functions and support vector machine models in GIS. *IEEE J. Sel. Top. Appl. Earth Obs. Remote Sens.* **2014**, *8*, 674–690. [[CrossRef](#)]
51. Cox, D.R. The regression analysis of binary sequences. *J. R. Stat. Soc. Ser. B Stat. Methodol.* **1958**, *20*, 215–232. [[CrossRef](#)]
52. Pepe, M.S.; Longton, G.; Janes, H. Estimation and comparison of receiver operating characteristic curves. *Stata J.* **2009**, *9*, 1–16. [[CrossRef](#)]

53. Corsini, A.; Mulas, M. Use of ROC curves for early warning of landslide displacement rates in response to precipitation (Piagneto landslide, Northern Apennines, Italy). *Landslides* **2017**, *14*, 1241–1252. [[CrossRef](#)]
54. Nadimi-Shahraki, M.H.; Zamani, H.; Asghari Varzaneh, Z.; Mirjalili, S. A systematic review of the whale optimization algorithm: Theoretical foundation, improvements, and hybridizations. *Arch. Comput. Methods Eng.* **2023**, *30*, 4113–4159. [[CrossRef](#)] [[PubMed](#)]
55. Ha, J.; Kang, J.E. Assessment of flood-risk areas using random forest techniques: Busan Metropolitan City. *Nat. Hazards* **2022**, *111*, 2407–2429. [[CrossRef](#)]
56. Khan, T.A.; Shahid, Z.; Alam, M.; Su'ud, M.; Kadir, K. Early flood risk assessment using machine learning: A comparative study of svm, q-svm, k-nn and lda. In Proceedings of the 2019 13th International Conference on Mathematics, Actuarial Science, Computer Science and Statistics (MACS), Karachi, Pakistan, 14–15 December 2019; pp. 1–7.
57. Lee, J.; Kim, B. Scenario-based real-time flood prediction with logistic regression. *Water* **2021**, *13*, 1191. [[CrossRef](#)]

**Disclaimer/Publisher's Note:** The statements, opinions and data contained in all publications are solely those of the individual author(s) and contributor(s) and not of MDPI and/or the editor(s). MDPI and/or the editor(s) disclaim responsibility for any injury to people or property resulting from any ideas, methods, instructions or products referred to in the content.